

Semiclassical Monte Carlo Model for In-Plane Transport of Spin-Polarized Electrons in III-V Heterostructures

Semion Saikin^{a,b,c}, Min Shen^a, Ming-C. Cheng^a and Vladimir Privman^{a,b}

^a*Center for Quantum Device Technology*

^a*Department of Electrical and Computer Engineering and*

^b*Department of Physics, Clarkson University*

Potsdam, New York 13699-5720, USA

^c*Department of Physics,*

Kazan State University, Kazan, Russian Federation

Abstract

We study the in-plane transport of spin-polarized electrons in III-V semiconductor quantum wells. The spin dynamics is controlled by the spin-orbit interaction, which arises via the Dresselhaus (bulk asymmetry) and Rashba (well asymmetry) mechanisms. This interaction, owing to its momentum dependence, causes rotation of the spin polarization vector, and also produces effective spin dephasing. The density matrix approach is used to describe the evolution of the electron spin polarization, while the spatial motion of the electrons is treated semiclassically. Monte Carlo simulations have been carried out for temperatures in the range 77-300 K and electric fields of order 2-4 kV/cm.

I. Introduction.

Promising applications of spintronics for novel device structures [1-5] have stimulated much interest in spin polarized transport. Many devices utilizing spin-dependent phenomena have been proposed recently [6-14]. At the present time, there are numerous difficulties with control of spin polarized current. Recent experimental advances [2] have allowed generation of spin polarization of conduction electrons in bulk semiconductors and in two-dimensional semiconductor structures. At room temperatures, spin polarization can be maintained for up to 1-2 nanoseconds.

Experimental investigations of spin polarized transport in semiconductors can be divided into three main areas: injection and detection of spin polarized current, spin relaxation of conduction electrons, and coherent spin dynamics.

Among few methods to create electron spin polarization in semiconductors [15-18], the electrical spin injection from magnetic contacts [17,18] is the most promising. However, the main difficulty of this approach has been in the correct band matching at the interface of magnetic material - semiconductor [19,20]. Also, the all-electrical experiments on the detection of spin injection are complicated by additional spin independent effects, which are difficult to separate from spin-dependent phenomena [21]. Thus, the recently reported values of the experimentally achieved spin polarization at room temperature have varied from 1-2% [22] up to 30-35% [23,24]. At low temperatures, $T \sim 4.2$ K, the polarization of the electrons injected from magnetic semiconductor contacts is appreciably higher and reaches the values of 50-80% [25,26].

The optical electron spin polarization and detection methods [16] are perhaps less applicable in the device design, but they have been very useful in investigations of electron spin dynamics, due to high efficiency of spin polarization at room temperature (more than 50%) and high sensitivity of measurement. Spin relaxation in semiconductor heterostructures has been studied extensively by the methods of ultrafast spin-sensitive spectroscopy [27-31]. At room temperature, the observed spin relaxation time varies widely, from less than 1 ps for structures with large spin-orbit interaction [27], up to 1 ns [28] for GaAs/AlGaAs quantum wells (QW) with the suppressed Dyakonov-Perel relaxation mechanism [32].

The spin-lattice relaxation of conduction electrons at high temperatures is dominated by several mechanisms arising from spin-orbit coupling. Their relative strength is determined by many different factors, some of which are established during the growth of the heterostructure and can not be well controlled. While for n-doped GaAs/AlGaAs QWs with (001) growth orientation the main relaxation mechanism at room temperature is Dyakonov-Perel [30], spin relaxation in narrow band gap (InGaAs/InP, InGaAs/InAlAs) heterostructures has no single explanation due to more complicated spin-orbit interactions [29,31].

Generally, the electron spin dynamics is controlled by external magnetic field, local magnetic fields produced by magnetic impurities and nuclei, and spin orbit interaction. In comparison with the electron spin transport model for ferromagnetic structures, which can be described in the two-current model [33], for nonmagnetic bulk semiconductors and semiconductor heterostructures the spin-orbit term is significant. This effect has been investigated by the analysis of Shubnikov-de Haas oscillations of magnetoresistance in strong magnetic fields [34,35] and of weak antilocalization in nearly-zero fields [36-38]. The tuning of the spin-orbit coupling constant by the gate voltage, which was proposed for current modulation in the spin-FET [6], has been demonstrated recently for InGaAs/InAlAs asymmetric QWs [35,39].

In the low-temperature and low-voltage regime, the value of the spin mean free path in bulk GaAs can reach few μm [40,41], which is much larger than industrially achievable device size [42]. The above overview of selected promising experimental results for spintronics device development, suggests that it is timely to develop device-modeling approaches incorporating spin polarization effects.

For low temperatures and low applied voltage, the single-particle ballistic models have been utilized [13,43,44]. Many of the existing semiclassical models have been developed along the lines of the earlier models used for ferromagnetic layered structures [33]. They are primarily of the drift-diffusion category, where the spin-up and spin-down electrons are described by charge- and spin-density conservation equations [45-47]. These models thus ignore quantum coherence effects of possible superposition of spin-up and spin-down states. For semiconductors, drift-diffusion models should be applicable for low electric fields only; some non-linear effects have been observed experimentally [20,41]. In addition, these models are not valid in small semiconductor devices and/or in fast-dynamics situations. For hot-electron spin-polarized transport, the coupled Boltzmann equations with only spin-up and spin-down states [48], or additionally including superimposed up-down states [49,50], have been considered.

The spin relaxation of conduction electrons and their spatial motion can not be separated exactly. However, in some drift-diffusion approximations, it can be shown that spin polarization of the electron gas decays exponentially in time in accordance with the spin-relaxation Bloch equations [51,52] with characteristic times T_1 and T_2 . It is

reasonable to assume, in analogy with the energy and momentum relaxation times [53] in energy-balance or hydrodynamic models for semiconductor devices, that these parameters will depend on the electron temperature, T_e , and, possibly, some other variables, $T_1(T_e, \dots)$, $T_2(T_e, \dots)$ [54]. Monte Carlo simulation including the electron spin state [55,56] can be useful for spin-dynamics modeling in the non-linear regime and extraction of such parameters. In this work, we utilize the Monte Carlo approach to simulate spin polarized transport in asymmetric QWs for intermediate values of electric fields ($\sim 2\text{-}4 \text{ kV/cm}$) for temperatures $T = 77\text{-}300 \text{ K}$.

II. Semiclassical density matrix approach to spin polarized electron transport.

Monte Carlo approach to Boltzmann equation for non-stationary electron transport has been widely used for modeling of submicrometer and deep-submicrometer devices. Here, we incorporate the description of the electron spin dynamics in a standard semiclassical Monte Carlo formalism [57,58]. The effective single-electron Hamiltonian with the spin-orbit interaction term is

$$H = H_0 + H_{\text{SO}}(\sigma, \mathbf{k}) . \quad (1)$$

H_0 is the self-consistent single electron Hamiltonian in the Hartree approximation, including also interactions with phonons and static imperfections. Inside the QW, this can be written as

$$H_0 = -\frac{\hbar^2}{2m^*} k^2 + e\gamma(\mathbf{r})(\mathbf{E}_{\text{ext}} \cdot \mathbf{r}) + H_{\text{e-ph}} + H_{\text{ph}} + V_{\text{imp}} . \quad (2)$$

The operator \mathbf{k} in the semiclassical treatment [57] is considered as momentum quantized in the z direction. We use the natural coordinate system, where x is the direction of the electric field along the channel, while z is orthogonal to the quantum well plane. Moreover, the axes are oriented along the principal crystal axes. The latter statement is important for the spin-orbit interaction terms which are dependent on the crystal orientation [32]. The screening factor $\gamma(\mathbf{r})$ accounts for the electron-electron interactions. It is determined by the appropriate Poisson equation [59]. The term V_{imp} describes ionized nonmagnetic impurities, QW roughness and other static imperfections of its structure. The terms labeled “e-ph” and “ph” represent the electron-phonon interaction and the phonon mode Hamiltonian. In the absence of external and local magnetic fields,

the electron magnetic interaction is only owing to the spin-orbit term $H_{\text{SO}}(\sigma, \mathbf{k})$ in Eq. (1). The main contributions to the spin-orbit interaction in an asymmetric III-V semiconductor QW structure are due to the Dresselhaus [60,32],

$$H_{\text{D}} = \beta \langle k_z^2 \rangle (k_y \sigma_y - k_x \sigma_x) , \quad (3)$$

and Rashba [61],

$$H_{\text{R}} = \eta (k_y \sigma_x - k_x \sigma_y) , \quad (4)$$

mechanisms, where the first equation as written, is applicable for narrow QWs, such that $k_x, k_y \ll \sqrt{\langle k_z^2 \rangle}$. For submicrometer devices with smooth potential, in the considered temperature regime ($T = 77\text{-}300$ K), we assume that the spatial electron transport is semiclassical and can be described by Boltzmann equation; see [59]. The electrons follow classical localized trajectories between the scattering events. The scattering rates are given by Fermi's Golden Rule, and the scattering events are instant. We also assume that the Elliott-Yafet spin scattering mechanism [62] is inefficient, i.e., that there are no electron spin flips accompanying momentum scattering. The back reaction of the electron spin evolution on the spatial motion is negligible owing to the small value of the electron momentum-state splitting due to spin-orbit interaction in comparison with its average momentum.

In Monte Carlo simulations, it is assumed that electrons propagate with constant velocity during the time δt , which is the smaller of the grid time step and time interval between two collisions. We can term such motion “free flight.” At the end of this time interval δt , the electron velocity is changed owing to acceleration in the electric field or due to scattering. Among many different scattering mechanisms [63], our Monte Carlo simulation has included charged impurity and phonon scatterings. The phonon bath in Eq. (2) is assumed to remain in thermal equilibrium with the constant lattice temperature T at all times. In the semiclassical Monte Carlo, the temperature is incorporated in the electron-phonon scattering rates [57,58].

For the description of the electron spin, we use the standard spin density matrix [64],

$$\rho_{\sigma}(t) = \begin{pmatrix} \rho_{\uparrow\uparrow}(t) & \rho_{\uparrow\downarrow}(t) \\ \rho_{\downarrow\uparrow}(t) & \rho_{\downarrow\downarrow}(t) \end{pmatrix} , \quad (5)$$

which is associated with the spin polarization vector as $S_\zeta(t) = \text{Tr}(\sigma_\zeta \rho_\sigma(t))$, where $\zeta = x, y, z$. For each “free flight” time interval, δt , the spin density matrix evolves according to

$$\rho_\sigma(t + \delta t) = e^{-iH_{\text{so}}\delta t/\hbar} \rho_\sigma(t) e^{iH_{\text{so}}\delta t/\hbar}. \quad (6)$$

This is equivalent to the rotation of the spin polarization vector about the effective magnetic field determined by the direction of the electron momentum. The exponential operators in Eq. (6) can be written as (2×2) scattering matrices,

$$e^{-iH_{\text{so}}\delta t/\hbar} = \begin{pmatrix} \cos(|\alpha|\delta t) & i\frac{\alpha^2}{|\alpha|^2}\sin(|\alpha|\delta t) \\ i\frac{(\alpha^*)^2}{|\alpha|^2}\sin(|\alpha|\delta t) & \cos(|\alpha|\delta t) \end{pmatrix}, \quad (7)$$

and Hermitean conjugate of Eq. (7) for operator $e^{iH_{\text{so}}\delta t/\hbar}$. Here α is determined by the spin-orbit interaction terms, Eqs. (3,4),

$$\alpha = 1/\hbar \left[(\eta k_y - \beta \langle k_z^2 \rangle k_x) + i(\eta k_x + \beta \langle k_z^2 \rangle k_y) \right]. \quad (8)$$

During the “free flight,” the spin dynamics of a single electron spin is coherent; see Eq. (6). However, stochastic momentum fluctuations during the scattering events, produce distribution of spin states, thus causing effective dephasing at times $t > 0$. The spin polarization, $\langle S_\zeta \rangle$, of the current can be obtained by averaging S_ζ over all the electrons in a small volume dv , which is located at position \mathbf{r} , at time t . The absolute value of the average spin polarization vector is in the range $|\langle \mathbf{S} \rangle| \leq 1$. If $|\langle \mathbf{S} \rangle|$ is equal 1, the electric current is completely spin polarized. The components $\langle S_\zeta \rangle$ define the orientation of the spin polarization, and evolution of the spin polarization vector may be viewed as coherent motion (rotation) and depolarization (reduction of magnitude).

III. Model and simulation results.

We have applied the model of spin polarized current, described in the preceding section, to simulation of electron transport in a single QW. Here, we utilize the asymmetric QW architecture in the one-subband approximation, which is a simplified model of $\text{In}_{0.47}\text{Al}_{0.53}\text{As}/\text{In}_{0.48}\text{Ga}_{0.52}\text{As}/\text{In}_{0.47}\text{Al}_{0.53}\text{As}$ heterostructures used in experiments probing

the spin-orbit coupling effects [35]; see Figure 1. Parameters of the confining potential and spin-orbit coupling constants, used in our simulations, are given in Table I. The Rashba and Dresselhaus coupling constants have been adopted from Refs. [35] and [65], respectively.

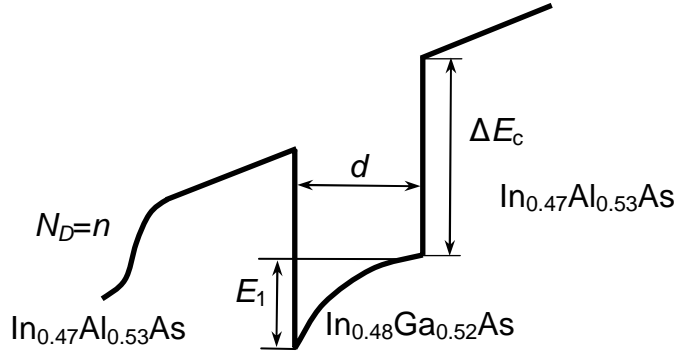


Figure 1. Model of the confining potential in the asymmetric $\text{In}_{0.47}\text{Al}_{0.53}\text{As}/\text{In}_{0.48}\text{Ga}_{0.52}\text{As}/\text{In}_{0.47}\text{Al}_{0.53}\text{As}$ quantum well.

Table I. Parameters of the confining potential and spin-orbit interaction coupling constants, where n is the equilibrium electron density, while the other quantities shown, are defined in Figure 1 or Section II.

d , nm	ΔE_c , eV	n , cm^{-2}	E_1 , eV	$\langle k_z^2 \rangle^{\frac{1}{2}}$, nm^{-1}	η , $\text{eV}\cdot\text{\AA}$	β , $\text{eV}\cdot\text{\AA}^3$
20	0.56	1×10^{12}	0.20	0.21	0.074	32.20

The ratio of the expectation values for the Dresselhaus and Rashba energy terms, Eqs. (3,4), is $E_R / E_D \approx 5.3$, which means that the Rashba term is dominant both for the coherent polarization-rotation dynamics and for depolarization. In our simulations, the device length was taken $l = 0.55 \mu\text{m}$, and infinite width was assumed. The material and scattering-rate parameters were taken from [59,63]. The total number of particles in the

channel was $N=55000$ and the grid time step was $\delta t_{grid} = 1$ fsec. To achieve the steady-state transport regime, we ran the simulation program for 20000 time steps, and collected data only during the last 2000 time steps. The simulations were carried out for temperatures $T = 77\text{-}300$ K and applied drain-source voltage $V_{DS} = 0.1\text{-}0.25$ V, which creates the in-channel electric field of the order of 2-4.5 kV/cm. The following boundary conditions were assumed: thermalized electrons were injected at the left boundary, with 100% initial spin polarization, and drained at the right boundary, with any spin polarization.

In the simulated device structure, the electron transport is non-equilibrium; see Figure 2. Evident velocity overshoot and other sharp features are observed due to a sudden increase in the electric field near the injecting boundary at all applied voltages. The electron average energy in the two-dimensional quantum well includes the drift and thermal energies:

$$\langle E \rangle = \frac{1}{2} m^* \langle \mathbf{v} \rangle^2 + kT_e . \quad (9)$$

Near the boundary at $x = 0$, where electrons are just injected, the thermal energy kT_e is dominant. Due to the finite scattering rate ($\sim 10^{-13}$ sec $^{-1}$), ballistic motion is observed in Figure 2a for distances as small as 0.01 μm , where average velocity increases considerably. This results in a sudden decrease in the ratio between the thermal and drift energies, as seen in Figure 2d, and leads to an abrupt increase in average energy, shown in Figure 2b. After the ballistic region, electrons suffer strong scattering that randomizes momentum and gives rise to velocity overshoot. In order to maintain the current continuity, electron concentration markedly drops at the location of the velocity overshoot; see Figure 2c.

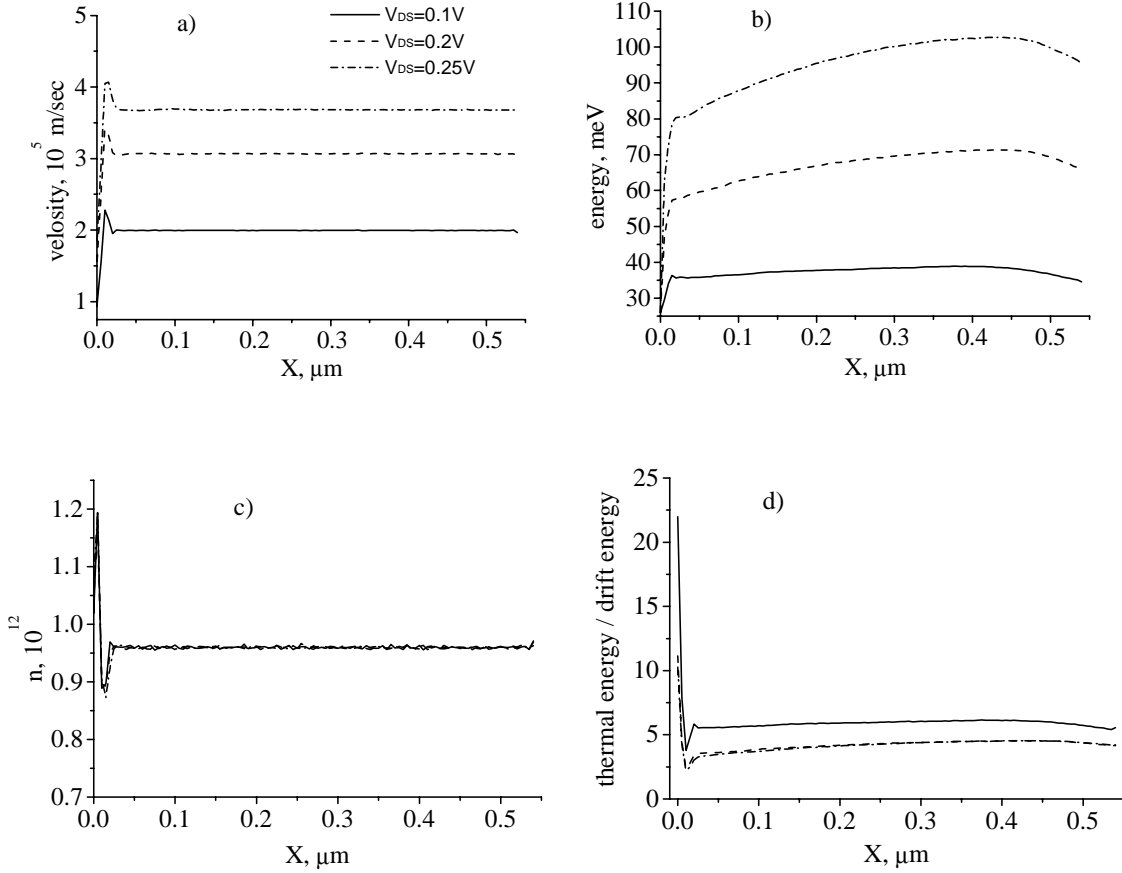


Figure 2. The electron transport parameters: a) drift velocity, b) average energy, c) electron concentration in the channel, and d) electron thermal energy as compared to their drift energy, as functions of x , at $T = 300$ K and $V_{DS} = 0.1\text{-}0.25$ V.

We calculate the evolution of the current's spin polarization for three initial polarizations: along the positive x , y and z directions. The corresponding initial single-electron density matrixes are,

$$\rho_x(0) = \frac{1}{2} \begin{pmatrix} 1 & 1 \\ 1 & 1 \end{pmatrix}, \quad \rho_y(0) = \frac{1}{2} \begin{pmatrix} 1 & -i \\ i & 1 \end{pmatrix}, \quad \rho_z(0) = \begin{pmatrix} 1 & 0 \\ 0 & 0 \end{pmatrix}. \quad (10)$$

Due to the symmetry of Rashba spin-orbit interaction term, Eq. (4), the spin polarization of the electrons, which propagate collectively in the x direction, will rotate about the y axis. This is shown in Figure 3, where, from now on, we omit the angular brackets that indicate averaging. The Dresselhaus term, Eq. (3), causes rotation about the x axis. Small

admixture of the later mechanism leads to the variation of the y projection of the spin polarization (Figures 3a, 3c), and of the x and z projections (Figure 3b), depending on the initial spin orientation.

The observed decay of the spin polarization occurs by dephasing owing to the electron momentum scattering events. Random momentum fluctuations, which are described by the electron thermal energy, produce an effective depolarization mechanism. The initial spin polarization drop in Figure 3, could be attributed to the effect of the high electron thermal energy in comparison with the drift energy, see Figure 2d. This effect can be clearly observed in Figure 4c, where the drop of the spin polarization near $x = 0$ is smaller for lower temperatures.

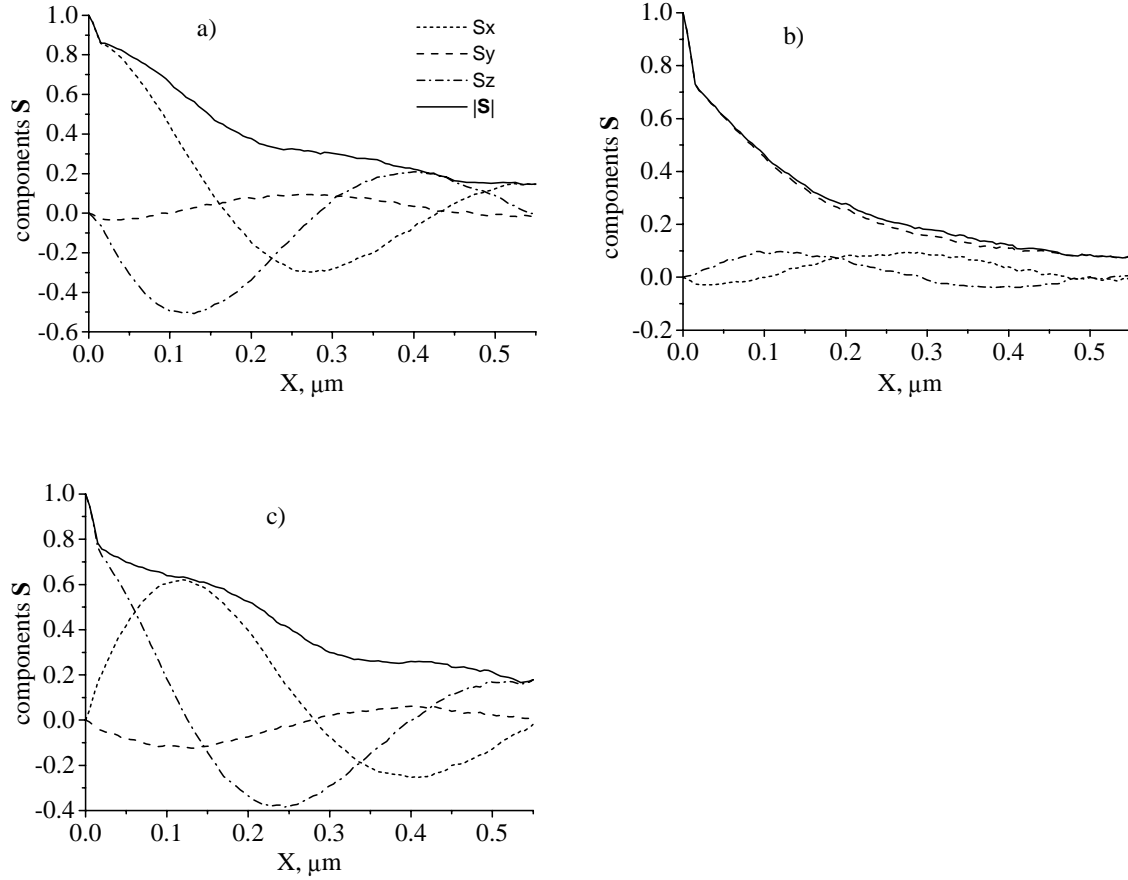


Figure 3. Evolution of the electron spin polarization \mathbf{S} , for $V_{\text{DS}} = 0.1$ V, at room temperature (300 K) for three different initial orientations of the spin polarization, along the positive a) x -, b) y -, c) z -axis.

Furthermore, Figure 4b shows that this drop is evidently less pronounced at higher applied voltage that enhances the drift velocity and relatively weakens the effect of the random momentum fluctuations. Moreover, in the considered model, the electron spin evolves between scattering events, and we expect to have complex dependence of the spin depolarization on the momentum scattering rate [32]. The initial drop could also be an artifact of the “free flight” assumption for regimes with strong acceleration.

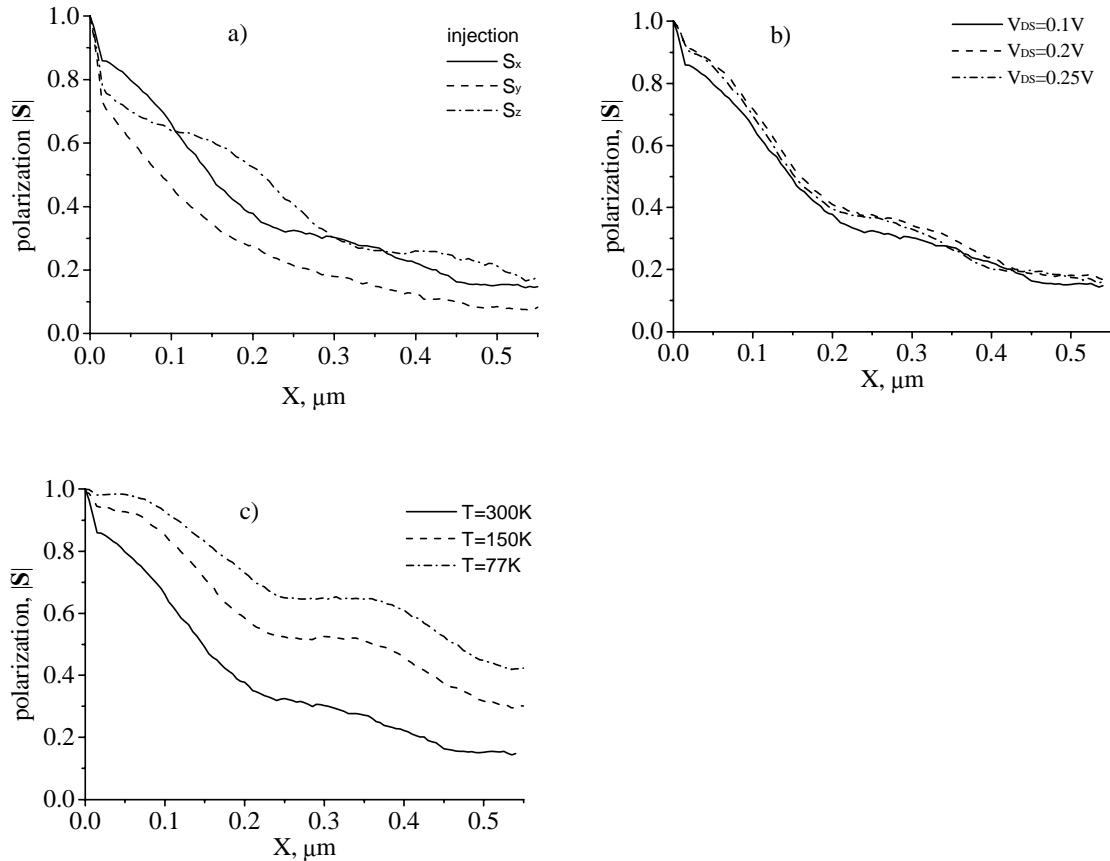


Figure 4. Spin depolarization effect for a) different orientations of the initial polarization, $T = 300$ K, $V_{DS} = 0.1$ V; b) different values of applied voltage, $T = 300$ K, initial polarization $S_x = 1$; c) different temperatures, initial polarization $S_x = 1$, $V_{DS} = 0.1$ V.

The depolarization rate in our model is asymmetric in the spin orientation. For example, the term proportional to $k_y \sigma_x$ in the Rashba spin-orbit interaction, Eq. (4), produces the

depolarization of the S_y and S_z components, due to the fluctuating k_y [6], but does not influence the S_x component of the spin polarization. The depolarization rate owing to the Rashba interaction is suppressed for an S_x -polarized current in comparison with S_y and S_z . This effect can be seen in Figure 4a.

It is interesting that, as shown in Figure 4b, the spin polarization at room temperature is not sensitive to the applied voltage in the investigated regime. Higher applied voltage, which leads to considerably larger drift velocity, only slightly increases the spin-dephasing length. The change of the spin polarization at higher applied voltage is minimized by the increase in mean energy that in turn increases the scattering probability. For lower temperatures, this quasi-balance apparently breaks down. Sufficient reduction of the temperature can suppress the electron-phonon scattering mechanism to yield longer spin mean free path. The temperature effect on the spin polarization in the range $T = 77\text{-}300\text{ K}$ is shown in Figure 4c. The calculated values of the spin mean free path at $V_{DS} = 0.1\text{ V}$ are $L_x \sim 0.2\text{ }\mu\text{m}$ and $L_x \sim 0.55\text{ }\mu\text{m}$, for $T = 300\text{ K}$ and $T = 77\text{ K}$, respectively. These values are significantly smaller than those obtained for bulk GaAs in the low-temperature ($T \sim 9\text{ K}$) regime [40,41], $L_x > 4\text{ }\mu\text{m}$, which could be attributed to stronger scattering.

IV. Discussion.

The simulation model developed in this paper, includes the linear terms of the spin-orbit coupling, which determine the spin energy basis. The terms cubic in the components of the momentum \mathbf{k} in the Dresselhaus spin-orbit interaction [60], and external magnetic field, can produce additional spin dephasing [49]. The Elliot-Yafet spin-scattering mechanism can be efficient in narrow-gap heterostructures. It can be included in our simulation model as an additional spin-evolution process at momentum scattering events.

The single subband approximation can be questioned for considered values of applied voltage. For the confining potential used in the simulation, the estimated splitting between ground and first-excited subbands is $\Delta E_{12} \sim 60\text{--}70\text{ meV}$. The intersubband scattering becomes effective at kinetic energies near $\Delta E_{12} - \hbar\omega_{LO} \sim 35\text{ meV}$, when optical phonon absorption becomes possible. The strong scattering begins when the electron

energy is above $\Delta E_{12} + \hbar\omega_{LO} \sim 100$ meV, and emission of optical phonons becomes possible. According to Figure 2b, the average electron energy exceeds a minimum value for the intersubband scattering for $V_{DS} > 0.1$ V. Up to the energy value of 100 meV, intersubband scattering rate is much less than intrasubband scattering rate [59], and we can assume that the single subband approximation gives the qualitatively correct description up to the $V_{DS} = 0.25$ V. For low temperatures, the average energy is reduced due to the condition of initial thermalization, Figure 5a, but, on the other hand, the electron-phonon scattering is suppressed, resulting in the energy increase, see Figure 5b. In comparison with the data shown in Figure 2b, the maximum value of the average electron energy for $V_{DS} = 0.2$ V is nearly the same. As a result, it is difficult to improve the validity of the single subband model for $V_{DS} > 0.2$ V by reducing the temperature. For different subbands, the spin-coupling constants are different, and it is likely that the spin dephasing will be even stronger if the intersubband scattering is incorporated.

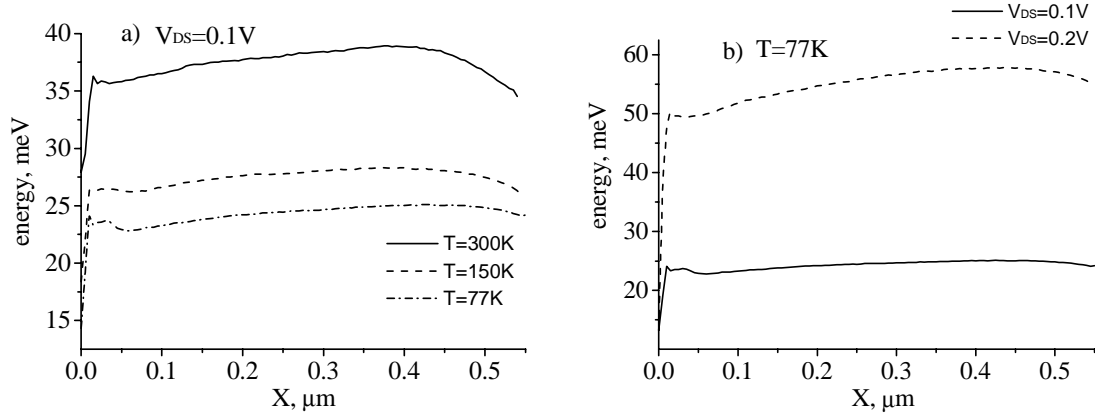


Figure 5. The average electron energy as function of a) temperature; b) applied voltage.

In conclusion, we have developed a semiclassical Monte Carlo model incorporating the linear terms of the Dresselhaus and Rashba spin-orbit coupling mechanisms for spin-polarized electron transport in III-V heterostructures. This approach can be used for simulation of non-equilibrium spin-dependent phenomena in spintronics devices. We reported results for the evolution of the spin polarization in a single quantum well at several temperatures and intermediate, $\sim 2\text{-}4$ kV/cm, electric fields. The estimated spin

depolarization length is in order of 0.2 μm , consistent with the presently available experimental evidence.

We thank Professors A. Shik and I. D. Vagner for helpful discussions. This research was supported by the National Security Agency and Advanced Research and Development Activity under Army Research Office contract DAAD-19-02-1-0035, and by the National Science Foundation, grants DMR-0121146 and ECS-0102500.

References.

1. S. Das Sarma, J. Fabian, X. Hu, I. Zutic, *IEEE Trans. Magn.* **36**, 2821 (2000).
2. S. A. Wolf, D. D. Awschalom, R. A. Buhrman, J. M. Daughton, S. von Molnar, M. L. Roukes, A. Y. Chtchelkanova, D. M. Treger, *Science* **294**, 1488 (2001).
3. S. Das Sarma, *Am. Sci.* **89**, 516 (2001).
4. D. D. Awschalom, M. E. Flatte, N. Samarth, *Sci. Am.* **286**, 66 (2002).
5. I. Zutic, *J. Supercond.* **15**, 5 (2002).
6. S. Datta, B. Das, *Appl. Phys. Lett.* **56**, 665 (1990).
7. B. E. Kane, L. N. Pfeiffer, K. W. West, *Phys. Rev. B* **46**, 7264 (1992).
8. M. Johnson, *Science*, **260**, 320 (1993).
9. M. E. Flatte, G. Vignale, *Appl. Phys. Lett.* **78**, 1273 (2001).
10. I. Zutic, J. Fabian, S. Das Sarma, *Appl. Phys. Lett.* **79**, 1558 (2001).
11. C. Ciuti, J. P. McGuire, L. J. Sham, preprint cond-mat/0205651 at www.arXiv.org (2002).
12. T. Koga, J. Nitta, H. Takayanagi, *Phys. Rev. Lett.* **88**, 126601 (2002).
13. X. F. Wang, P. Vasilopoulos, F. M. Peeters, *Phys. Rev. B* **65**, 165217 (2002).
14. R. G. Mani, W. B. Johnson, V. Narayanamurti, V. Privman, Y.-H. Zhang, *Physica E* **12**, 152 (2002).
15. S. F. Alvarado, P. Renaud, *Phys. Rev. Lett.* **68**, 1387 (1992).
16. J. Kikkawa, D. D. Awschalom, *Science* **277**, 1284 (1997).
17. M. Oestreich, J. Hubner, D. Hagele, P. J. Klar, W. Heimbrodt, W. W. Ruhle, D. E. Ashenford, B. Lunn, *Appl. Phys. Lett.* **74**, 1251 (1999).

18. Y. Ohno, D. K. Young, B. Beschoten, F. Matsukura, H. Ohno, D. D. Awschalom, *Nature* **402**, 790 (1999).

19. G. Schmidt, D. Ferrand, L. W. Molenkamp, A. T. Filip, B. J. van Wees, *Phys. Rev. B* **62**, R4790 (2000).

20. G. Schmidt, C. Gould, P. Grabs, A. M. Lunde, G. Richter, A. Slobodskyy, L. W. Molenkamp, preprint cond-mat/0206347 at www.arxiv.org (2002).

21. A. T. Filip, B. H. Hoving, F. J. Jedema, B. J. van Wees, B. Dutta, S. Borghs, *Phys. Rev. B* **62**, 9996 (2000).

22. K. H. Ploog, *J. Appl. Phys.* **91**, 7256 (2002).

23. P. R. Hammar, M. Johnson, *Phys. Rev. Lett.* **88**, 066806 (2002).

24. A. T. Hanbicki, B. T. Jonker, G. Itskos, G. Kioseoglou, A. Petrou, *Appl. Phys. Lett.* **80**, 1240 (2002).

25. R. Fiederling, M. Keim, G. Reuscher, W. Ossau, G. Schmidt, A. Waag, L. W. Molenkamp, *Nature* **402**, 787 (1999).

26. B. T. Jonker, Y. D. Park, B. R. Bennett, H. D. Cheong, G. Kioseoglou, A. Petrou, *Phys. Rev. B* **62**, 8180 (2000).

27. K. C. Hall, S. W. Leonard, H. M. van Driel, A. R. Kost, E. Selvig, D. H. Chow, *Appl. Phys. Lett.* **75**, 4156 (1999).

28. Y. Ohno, R. Terauchi, T. Adachi, F. Matsukura, H. Ohno, *Phys. Rev. Lett.* **83**, 4196 (1999).

29. A. Tackeuchi, T. Kuroda, Sh. Muto, O. Wada, *Physica B* **272**, 318 (1999).

30. A. Malinowski, R. S. Britton, T. Grevatt, R. T. Harley, D. A. Ritchie, M. Y. Simmons, *Phys. Rev. B* **62**, 13034 (2000).

31. T. Adachi, Y. Ohno, R. Terauchi, F. Matsukura, H. Ohno, *Physica E* **7**, 1015 (2000).

32. M. I. Dyakonov, V. Yu. Kachorovskii, *Sov. Phys. Semicond.* **20**, 110 (1986).

33. A. Fert, I. A. Campbell, *J. Physique (Paris), Colloq.* **32**, C1 (1971).

34. B. Das, D. C. Miller, S. Datta, R. Reifenberger, W. P. Hong, P. K. Bhattacharya, J. Singh, M. Jaffe, *Phys. Rev. B* **39**, 1411 (1989).

35. J. Nitta, T. Akazaki, H. Takayanagi, *Phys. Rev. Lett.* **78**, 1335 (1997).

36. P. D. Dresselhaus, C. M. A. Papavassiliou, R. G. Wheeler, R. N. Sacks, *Phys. Rev. Lett.* **68**, 106 (1992).

37. W. Knap, C. Skierbiszewski, A. Zduniak, E. Litwin-Staszewska, D. Bertho, F. Kobbi, J. L. Robert, G. E. Pikus, F. G. Pikus, S. V. Iordanskii, V. Mosser, K. Zekentes, Yu. B. Lyanda-Geller, *Phys. Rev. B* **53**, 3912, (1996).

38. T. Koga, J. Nitta, T. Akazaki, H. Takayanagi, *Phys. Rev. Lett.* **89**, 046801 (2002).

39. Y. Sato, T. Kita, S. Gozu, S. Yamada, *Physica E* **12**, 399 (2002).

40. D. Hagele, M. Oestreich, W. W. Ruhle, N. Nestle, K. Eberl, *Appl. Phys. Lett.* **73**, 1580 (1998).

41. H. Sanada, I. Arata, Y. Ohno, Z. Chen, K. Kayanuma, Y. Oka, F. Matsukura, H. Ohno, *Appl. Phys. Lett.* **81**, 2788 (2002).

42. L. Geppert, *IEEE Spectrum*, October 2002, page 28.

43. F. Mireles, G. Kirczenow, *Phys. Rev. B* **64**, 024426 (2001).

44. Th. Schapers, J. Nitta, H. B. Heersche, H. Takayanagi, *Physica E* **13**, 564 (2002).

45. J. Fabian, I. Zutic, S. Das Sarma, *Phys. Rev. B* **66**, 165301 (2002).

46. G. Schmidt, L. W. Molenkamp, *Semicond. Sci. Tech.* **17**, 310 (2002).

47. Z. G. Yu, M. E. Flatte, preprint cond-mat/0206321 at www.arxiv.org (2002).

48. T. Valet, A. Fert, *Phys. Rev. B* **48**, 7099 (1993)

49. M. Q. Weng, M. W. Wu, preprint cond-mat/0209007 at www.arxiv.org (2002).

50. Y. Qi, S. Zhang, preprint cond-mat/0211674 at www.arxiv.org (2002).

51. W. H. Lau, J. T. Olesberg, M. E. Flatte, *Phys. Rev. B* **64**, 161301 (2001).

52. I. I. Puller, L. G. Mourokh, N. J. M. Horing, A. Yu. Smirnov, preprint cond-mat/0209296 at www.arxiv.org (2002).

53. Ming-C. Cheng, *J. Phys. D: Appl. Phys.* **32**, 3047 (1999).

54. N. S. Averkiev, L. E. Golub, M. Willander, *J. Phys.: Cond. Matt.* **14**, R271 (2002).

55. A. Bournel, P. Dollfus, S. Galdin, F.-X. Musalem, P. Hesto, *Solid State Comm.* **104**, 85 (1997).

56. A. Bournel, V. Delmouly, P. Dollfus, G. Tremblay, P. Hesto, *Physica E* **10**, 86 (2001).

57. K. Tomizawa, *Numerical Simulation of Submicron Semiconductor Devices* (Artech House, 1993).

58. C. Moglestue, *Monte Carlo Simulation of Semiconductor Devices* (London, Chapman & Hall, 1993).

59. V. V. Mitin, V. A. Kochelap, M. A. Stroscio, *Quantum Heterostructures*.

Microelectronics and Optoelectronics (Cambridge University Press, Cambridge, UK 1999).

60. G. Dresselhaus, Phys. Rev. **100**, 580 (1955).
61. Yu. Bychkov, E. I. Rashba, J. Phys. C **17**, 6039 (1984).
62. R. J. Elliott, Phys. Rev. **96**, 266 (1954).
63. M. V. Fischetti, S. E. Laux, *Damocles Theoretical Manual* (IBM Corporation, April 1995).
64. K. Blum, *Density Matrix Theory and Applications* (Plenum Press, New York, 1996).
65. M. Cardona, N. E. Christensen, G. Fasol, Phys. Rev. B **38**, 1806 (1988).